Journal of Renewable Materials

Tech Science Press

DOI: 10.32604/jrm.2024.050685

ARTICLE

Advanced Nanocomposite Arabic Gum Polyacrylic Acid Hydrogels for Flexible Supercapacitors

Borhan Albiss* **and Asala Saleh**

Nanotechnology Institute, Jordan University of Science and Technology, P.O. Box 3030, Irbid, 22110, Jordan

*Corresponding Author: Borhan Albiss. Email: baalbiss@just.edu.jo

Received: 13 February 2024 Accepted: 27 May 2024 Published: 21 August 2024

ABSTRACT

In this work, the fabrication and characterization of the nanocomposite hydrogel, as a solid electrode in electrochemical cell and gel electrolyte material using Indium titanium oxide/polyethylene terephthalate (ITO/PET) flexible substrate for double-layer supercapacitors have been reported. The nanocomposite hydrogel composed of Arabic gum (AG), Acrylic acid (AA), reduced graphene oxide (RGO), and silver nanoparticles (AgNPs) was fabricated via a physical cross-linked polymerization reaction, in which the ascorbic acid was used as a reducing agent to generate AgNPs and to convert Graphene oxide (GO) to RGO during the polymerization reaction. The morphology and structural characteristics of nanocomposite hydrogel were investigated using atomic force microscopy (AFM), scanning electron microscope (SEM), Fourier transfer infrared (FTIR), and X-ray fluorescence (XRF). Additionally, the effect of RGO and AgNPs on hydrogel stability was assessed through Thermogravimetric analysis (TGA) and differential scanning calorimetry (DSC), while its mechanical properties were studied using the nanoindentation test. Electrochemical impedance spectroscopy (EIS), and cyclic voltammetry (CV) were also conducted to study the electrochemical properties of the prepared hydrogel. The effects of AgNPs, RGO, and water content were all considered in the study of supercapacitor performance. The microstructural tests showed that the nanocomposite hydrogel has a relatively high swelling rate, which has a crucial effect on the capacitance. Furthermore, the effects of increasing AgNP concentration and water content in the hydrogel matrix showed a significant improvement in its electrochemical performance, compared with that for Arabic gum poly acrylic acid (AGPAA) hydrogel itself, were the specific capacitance exhibited a significant enhancement, converting from a low value to a substantially higher capacitance value. Moreover, when the nanocomposite hydrogel was used as the working electrode in an electrochemical cell with a hydrochloric acid (HCl) electrolyte solution, it exhibited good electrode performance. Additionally, using (ITO/PET) as a flexible substrate for nanocomposite hydrogel shows an improvement in their suitability for supercapacitor applications. Therefore, it is suggested that the fabricated hydrogel supercapacitor has potential applications in the field of renewable and clean energy harvesting.

KEYWORDS

Supercapacitor; energy harvesting; nanocomposite hydrogel; reduced graphene oxide

1 Introduction

The large development of industry has resulted in the consumption of natural fuel resources, contributing to an escalation in environmental pollution [1–4]. To address this challenge, there is a need to develop renewable, low-cost, and effective energy storage systems [5,6]. Among the various solutions, a flexible supercapacitor with sufficient energy storage has attracted the attention of the applications of wearable and flexible electronic devices. This interest is due to its high-performance attributes, represented by its fast charging-discharging ability, low cost, high specific power, and long cycle life. Furthermore, its high conductivity and stable mechanical properties make it an attractive choice for renewable energy solutions [5,7–9]. Recent progress in the supercapacitor field separates their performance based on the storage mechanisms into pseudo-capacitors and an electrostatic double layer (EDS) [10].

Pseudo-capacitor based on redox reactions between electrode materials to store energy. While the EDLC is the simplest and most commercially available supercapacitor, it stores energy based on electrolyte ion adsorption on the electrode surface [11–13]. Both transition metal oxides and conducting polymers are considered novel electrode materials for the enhancement of pseudo-capacitors, which show higher energy density compared with EDLC. Furthermore, the higher energy and power density increased researcher attention to the pseudo-capacitor method [14–16]. Electrode fabrication based on nano-structuring techniques has been employed to enhance the kinetics of charge transfer and increase the electrode material surface area. High specific surface area and the porosity of electrode materials play a key role in increasing EDLC capacitive performance, in addition to using carbon nanomaterials such as graphene and its derivatives, activated carbon, and carbon nanotubes in electrode fabrication to enhance their properties [13,17,18]. Recent literature reviews show the tendency of capacitive performance to find and understand the phenomenon of improving electrode materials and the importance of overcoming the challenges of supercapacitor technology in different applications, including renewable energy systems and energy storage [14,16].

Taking into account the electrolyte mode that could influence the capacitance, energy density, power density, or the voltage window. Reliability and resistance to corrosion and leakage, besides a lower ionic conductivity, make solid-gel electrolytes a good candidate for flexible energy storage devices compared to gel polymer electrolytes (GPE). The latter one has been introduced due to its environmental benefits, high ionic conductivity, high chemical stability, good mechanical properties, dimensional stability, and flexibility [6,19]. One of the most investigated flexible electrodes in electronic devices was indium tin oxide coated on polyethylene terephthalate (ITO/PET) [20].

The conductive and flexible nature of nanocomposite hydrogels makes them an ideal choice for flexible supercapacitors [8]. Hydrogel is a 3D network structure created by physical or chemical bonds between its neutral or synthetic polymers. The low conductivity of hydrogel and its poor mechanical properties, represented by its low toughness, tensile ability, and strength, will limit its use in several electronic device applications. Incorporating inorganic components, including a metal oxide, graphene and its derivatives, indium tin oxide (ITO), nanoparticles, and conductive polymers, into the hydrogel matrix addresses these limitations [21–25]. Graphene is one of the most promising materials in energy storage due to its excellent mechanical properties, large surface area, and high conductivity. Zhao et al. used P and N co-doped graphene to enhance the energy and power density of the supercapacitor, which resulted in high specific capacitance of the Zn-ion hybrid supercapacitor in $ZnSO_4$ solution. Ge et al. fabricated nitrogen-doped graphene coupled with an aligned polyaniline electrode (NG/PANI), which improved the electrochemical performance of supercapacitors compared with individual electrodes [26,27]. In addition, the presence of ions and inorganic compounds with high water content in the hydrogel network structure will help avoid the leakage of GPE, improve the conductivity of electrolytes,

and enhance hydrogel surface area and porosity [3,7,19,28–31]. Considerations for size, toughness, and anti-swelling performance are crucial in the development of flexible supercapacitors using conductive polymers like polyacrylic acid (PAA) and its composite with Arabic gum (AG). The addition of AG to the PAA matrix polymer enhances material properties due to its high mechanical properties, high contact area, thermal stability, and high energy storage, in addition to its chemical stability. Furthermore, polyvinyl alcohol and polyacrylic acid are commonly used in most electronic devices, like flexible supercapacitors [7,30,32].

Arabic gum (AG) is a highly branched natural polysaccharide, extracted from the acacia tree. It is comprised of arabinose residues, rhamnose, galactose, and glucuronic acid. This amorphous, odorless, and colorless resin has been used in wide applications in several fields due to its biocompatibility, high water solubility, nontoxicity, PH stability, and low viscosity compared with other polysaccharides [33–37]. Due to these properties, AG is widely used as a stabilizer, liquid flavor emulsion, and emulsifier, in addition to being used in several applications, including the food industry, textile industry, water treatment, and printing. Furthermore, AG can be used to build up copolymer hydrogel, improve hydrogel physiochemical properties, and work as a stabilizing and reductant for AgNPs [38–41].

The hydrogel matrix lacks good electrical conductivity, which limits its usage in flexible electrode devices. To resolve this issue, graphene, which has a large specific surface area and excellent electrical conductivity, can be easily integrated into a hydrogel matrix. The 2D mono-atomic layer of graphene enables active material to be loaded on its surface through chemical bonds or electrostatic interaction with oxygen functional groups [1,28,42,43]. The noble metals were introduced to enhance the electrical conductivity of the hydrogel matrix electrode. In this profile, the unique properties of silver nanoparticles (AgNPs), with their low cost and stability, have advantages compared to gold and platinum metals [44]. In particular, the high thermal stability and high conductivity of silver metal make it an important material for nanoparticle production. The addition of AgNPs to the hydrogel matrix will reduce polymer electrical resistance, enhance the optical and thermal properties of the hydrogel, and increase the specific capacitance and electrical conductivity of the prepared nanocomposite hydrogel to be used as a supercapacitor material [45–47].

In this work, the nanocomposite of Arabic gum polyacrylic acid tough hydrogel (RGO-AgNPs/AGPAA-hydrogel) was fabricated using a novel technique. The nanocomposite served as a separator and an electrolyte. Both solid gel and polymer gel electrolytes were fabricated based on RGO/AgNPs/AGPAA-hydrogel by an in-situ polymerization reaction. In this study, both ITO/PET and a flexible hydrogel were used to fabricate a flexible supercapacitor device, allowing it to bend or conform to diverse shapes. The nanocomposite is sandwiched between two conductive ITO/PET electrodes. The electrochemical impedance spectroscopy (EIS), cyclic voltammetry (CV), and electrochemical and mechanical characteristics of the composite hydrogel were thoroughly investigated.

2 Experiment Section

2.1 Materials

All materials used in this research were purchased from Sigma-Aldrich and were of analytical grade: Iron (iii) Chloride ($FeCl_3$), graphite (fine powder extra pure), Ascorbic Acid (VC), sulfuric acid (H_2SO_4, 96%), Arabic Gum (AG), sodium nitrates ($NaNO_3$), Acrylic Acid (AA), potassium permanganate ($KMnO_4$), hydrogen peroxide (H_2O_2, 30%), hydrochloric acid (HCl, 37%), silver nitrate ($AgNO_3$), and Ammonium Per Sulfate (APS).

2.2 Preparation of GO

Graphene oxide was synthesized using the modified Hummer method [48].

2.3 Preparation of RGO/AgNPs/AGPAA-Nanocomposite Hydrogels

1. GO was first dissolved in deionized water using ultrasonication. Then ascorbic acid was added slowly to convert GO to RGO.
2. Formation of AG-PAA-hydrogel: AG was dissolved completely in deionized water, then AA solvent was added slowly. After 10 min, $FeCl_3$ and APS were added to the hydrogel matrix. Then keep stirring at 40°C for 2 h [49].
3. Formation of RGO-AgNPs-AGPAA-hydrogel: The $AgNO_3$ and (1) solution were slowly added to the hydrogel matrix (2), and then it was allowed to stir at 90°C for 1 h. Fig. 1 shows the flowchart of the synthesis process of AGPAA nanocomposite hydrogel.

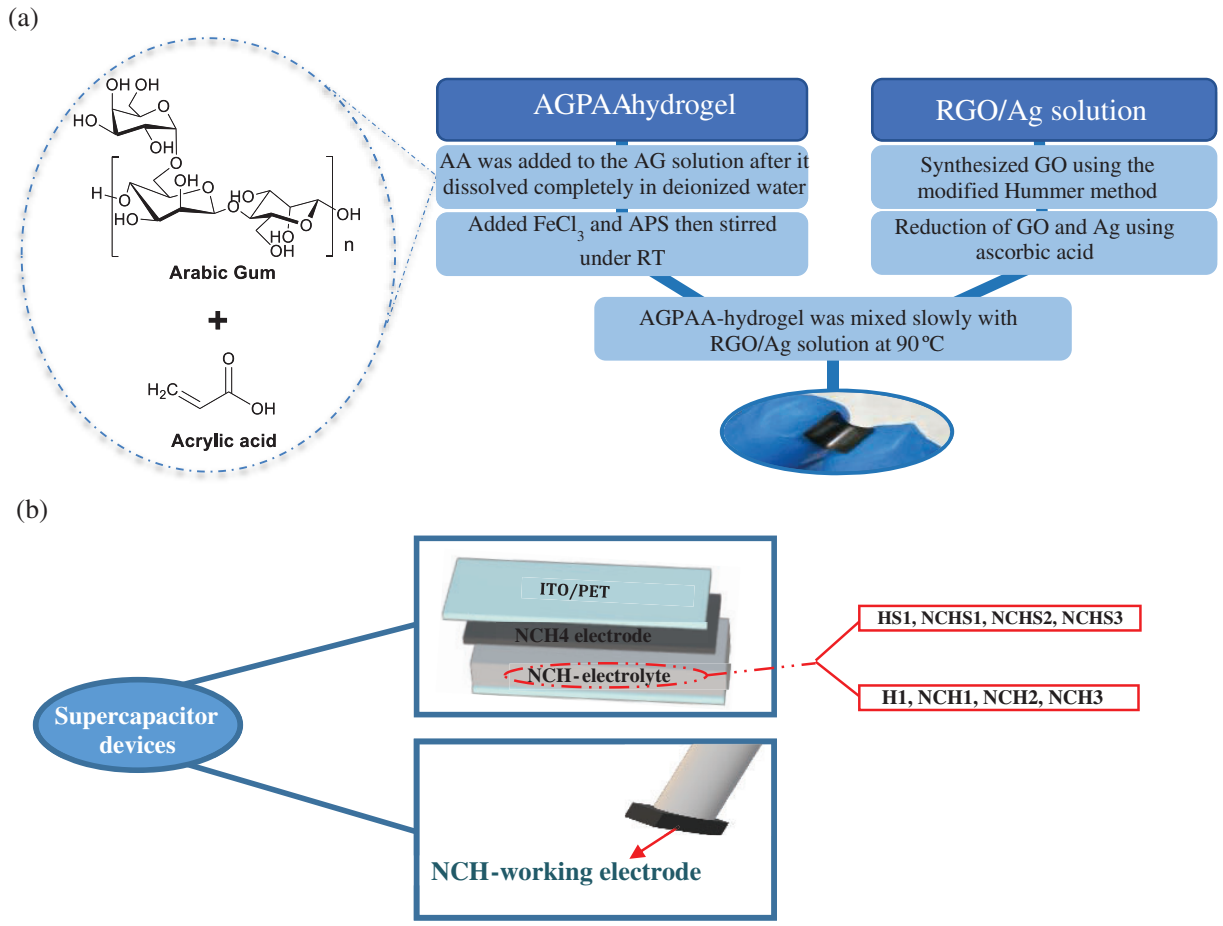

Figure 1: Flowchart of the (a) synthesis procedure of AGPAA nanocomposite hydrogel and (b) supercapacitor hydrogel devices

2.4 Preparation of the Hydrogel Supercapacitor

1. Hydrogel electrolyte gel: the hydrogel with 1.0% GO and several Ag concentrations was swelled in 10 mL of distilled water until the hydrogel size was fixed.
2. Solid-gel electrode: 10.0% of the AGPAA-hydrogel matrix was used to prepare nanocomposite hydrogel.

3. ITO/PET was used as a flexible substrate in the supercapacitor. A PET/ITO/solid-gel/hydrogel electrolyte/solid gel/ITO/PET double-sandwiched layer was used as a supercapacitor device. Fig. 1b shows the schematic diagram of the nanocomposite hydrogel devices.

Table 1 shows the AGPAA-hydrogel with a different concentration of AgNPs and RGO. The hydrogel was allowed to swell for 10 min to increase its water content. The effect of adding AgNPs and RGO on hydrogel properties was studied. In addition, the change in hydrogel electrochemical properties between two different hydrogel electrolyte types was instigated to study the effect of increasing water content inside a hydrogel matrix network.

Table 1: The AGPAA-hydrogel with different Ag and GO concentrations

Hydrogel code	%GO	$\%Ag^{+1}$
H1	0.00	0.00
NCH1	1.00	0.10
NCH2	1.00	0.50
NCH3	1.00	1.00
NCH4	32.0	32.0
HS1*	0.00	0.00
NCHS1*	1.00	0.10
NCHS2*	1.00	0.50
NCHS3*	1.00	1.00

Note: *: The sample was allowed to swell in distilled water until its size was fixed.

The H1, NCH2, and NCH3 hydrogels were used in a 3-electrode system with 0.6 M of aqueous hydrochloric acid (HCl) as the working electrode to study their electrochemical behavior (Fig. S1a). The Ag/AgCl was used as the reference electrode, while Pt foil was used as a counter electrode. As shown in the (Fig. S1b) the hydrogel supercapacitor sandwiched between two ITO/PET electrodes. The hydrogel was used as an electrolyte in the capacitor, while the NCH4 sample was used as a solid electrode. In this research, we study the effect of gel polymer electrolyte and solid polymer electrolyte on supercapacitor efficiency.

3 Results and Discussion

The surface morphology of the as-prepared hydrogel structure was mapped using SEM and AFM techniques (Fig. 2). The SEM images of H1 and NCH3 samples are illustrated in Figs. 2a,b. A high-porous structure of the hydrogel matrix H1 sample is supported by a volcano-like structure, as seen in Fig. 2a. The high porosity can enhance the mobility of ions and charge transfer within the electrolyte hydrogel due to its large surface area. Fig. 2b reveals the effect of additives of RGO and AgNPs on the internal structure and surface morphology of the hydrogel matrix, in addition to the presence of AgNPs on the NCH3 sample surface. The AgNPs embedded within the hydrogel exhibited a size distribution ranging from 20 to 50 nm. Fig. 2c shows AFM images in two- and three-dimensional modes of the NCH3 sample. The dispersed AgNP nanoparticles are shown on the surface of the NCH3. The roughness and the projected area of the NCH3 sample were found to be 145.62 nm and 99.6098 μm^2, respectively.

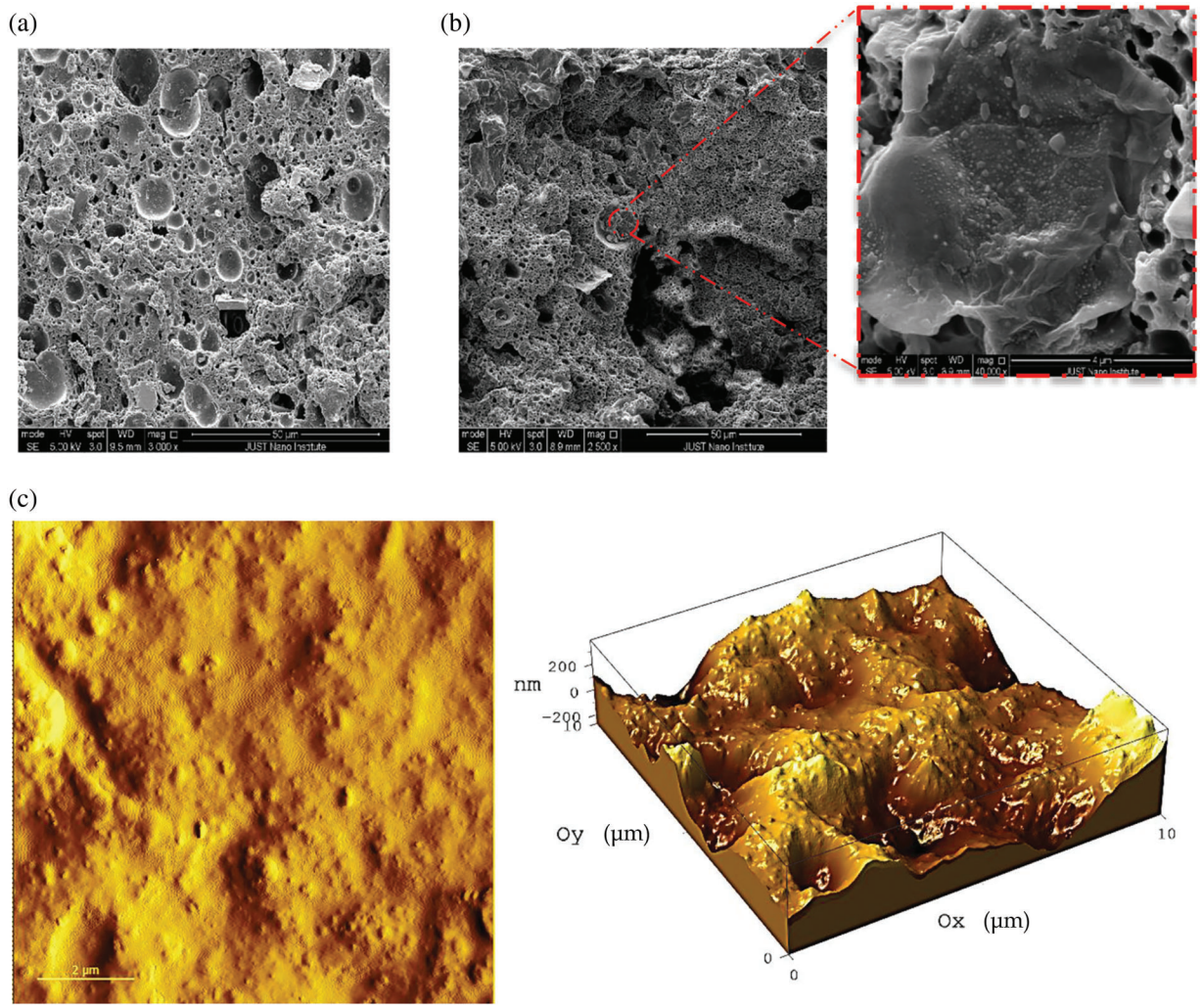

Figure 2: SEM images of (a) H1 and (b) NCH3 samples; (c) 2D and 3D AFM images of NCH3 samples

The FTIR spectra obtained for acrylic acid (AA) and Arabic gum (AG), in addition to the prepared hydrogels (H1, NCH3, and NCH4), are shown in Fig. 3. Fig. 3a shows a significant difference between the AA monomer, AG polymer, and H1 sample, in which many of the FTIR peaks on AA monomers disappeared from the H1 sample. The peak at 1685 cm^{-1} is assigned to C=C stretching vibration in AA that disappeared from the H1 sample, which reveals the successful formation of PAA. The peaks at 2932 and 2897 cm^{-1} are attributed to the sp^3 stretching vibration of the C-H group in the H1 sample and AG, respectively, with a highly intense peak compared with a tiny peak in the AA monomer. The peaks at 1711 and 1693 cm^{-1} represent the C=O stretching vibration of the H1 sample and AA monomer, respectively. Peaks from (1031–1072) cm^{-1} represent a C-O-C and C-O-H stretching vibration in the H1 sample and AG polymers; these peaks refer to the saccharide structure of hybrid hydrogel. The O-H stretching vibration of oxygen functional groups was found in the range of 3000–3500 cm^{-1}, with a significant difference in peak broadness between AA, AG, and the H1 sample due to the interaction between the prepared H1 sample hydroxyl group and Fe^{+3}. Also, the interactions between the oxygen functional groups, like the -OH group and C=O group in PAA-AG and PAA-PAA, will affect the broadness of the -OH stretching vibration in the H1 sample. Fig. 3b shows a significant difference in

hydrogel spectra as a result of the addition of RGO and AgNPs with different concentrations in both the NCH3 and NCH4 samples compared with the H1 sample. The peaks at 3789 and 3776 cm^{-1} refer to the -OH stretching vibration on H1 and NCH3 samples, which disappeared in the NCH4 sample. The board peaks at (3000–3500) cm^{-1} which refers to the -OH stretching vibration of alcohol that disappeared from the NCH4 sample. In the NCH3 sample, a peak at 2982 cm^{-1} that represents the C-H stretching vibration is absent from both the NCH4 and H1 samples. The absence of these peaks from the NCH4 sample may be related to the strong interaction between hydrogel functional groups and the additive (AgNPs and RGO) when a high concentration is used. In addition, these additives in the hydrogel matrix will affect the hydrogen and dipole bonding in the polymer network structure, which causes a change in peak intensity or appearance. The peaks from (1346–1348) cm^{-1} in both H1 and NCH3 samples represent the deformation vibration of the CH_3 group, where his peak disappeared from the NCH4 sample. The C-O stretching vibration at 1008 cm^{-1} in the H1 sample becomes very small in the NCH3 sample and disappears from the NCH4 sample, which shows the high effect of RGO concentration. Also, the change in C=O stretching vibration (1750–1660) cm^{-1} in carboxylic acid indicates the presence of RGO.

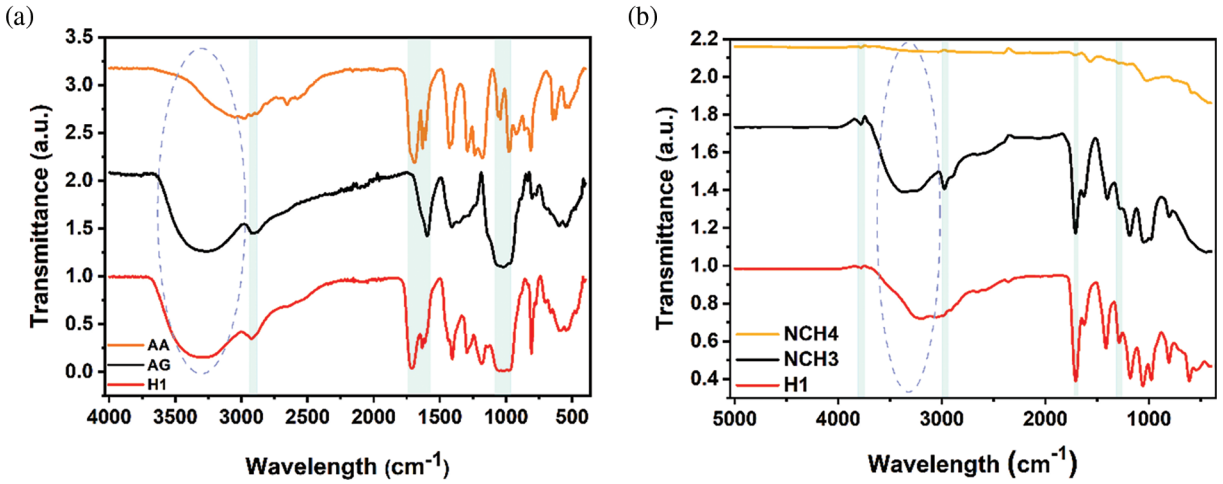

Figure 3: (a) FTIR spectrum fitting diagram of AA, AG, and H1 samples in 400–4000 cm^{-1}; (b) FTIR spectrum fitting diagram of H1, NCH3, and NCH4 samples in 500–5000 cm^{-1}

The thermal stability and crystallinity of the H1 and NCH3 samples were characterized by TGA and DSC analysis in their dry states. In the TGA, the thermal stability of the prepared hydrogel was tested. The H1 and NCH3 samples show two steps of weight loss. The T_e (extrapolated onset temperature) was used to compare the thermal stability of both samples. We can see the effect of added AgNPs and RGO on the hydrogel thermal stability; sample H1 shows more weight loss compared with the NCH3 sample behavior at different temperatures (Fig. 4a). The loss in weight after 200°C refers to removing water content and gases from the hydrogel matrix. Fig. 4b shows the DSC of the H1 and NCH3 dried samples. The crystallinity difference between samples refers to adding RGO and AgNPs to the hydrogel matrix. A small peak close to 90°C represents the loss of water and volatile content. The physical transition endothermic peaks are found close to 150°C and 190°C of the T_g and T_m values, respectively. The T_g value of the NCH3 sample shows a more intense peak compared with the H1 sample, which indicates the increase in water content inside the matrix structure, in addition to the effect of the RGO and AgNPs on increasing the porosity of the hydrogel. The H1 sample shows two intense peaks close to 200°C, while the small peak of the NCH3 sample is at 190°C; therefore, the difference in peak intensity between samples indicates the difference in sample crystallinity.

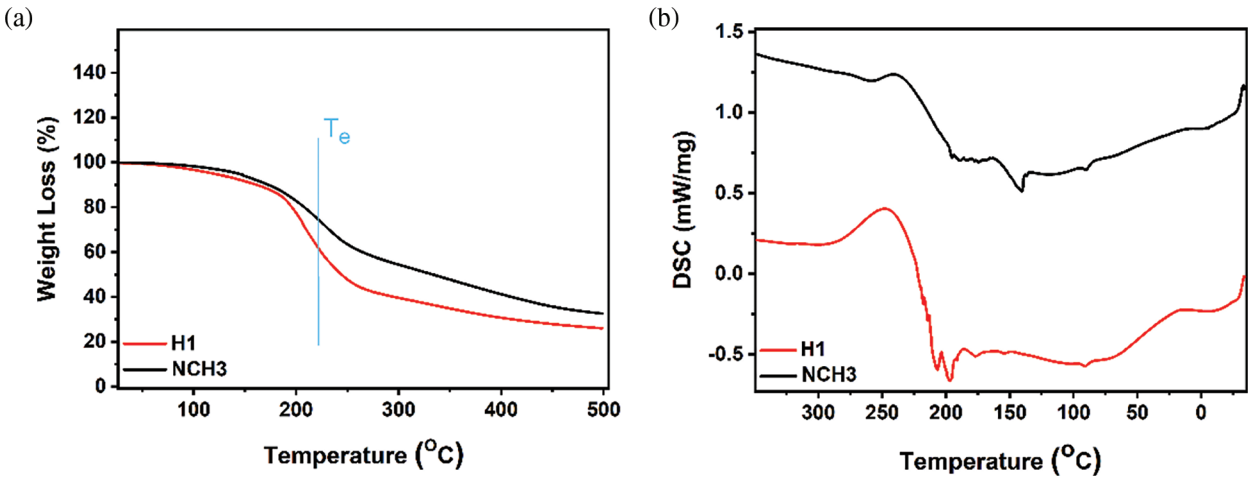

Figure 4: (a) TGA fitting diagram of H1 and NCH3 samples; (b) DSC fitting diagram of H1 and NCH3 samples

Fig. 5 shows the XRF analysis of nanocomposite hydrogel samples with different Ag concentrations. The increase in Ag concentration results in increasing peak intensity of the sample; the NCH4 sample shows a higher peak intensity compared with that of the NCH1 and NCH2 samples. The different number of peaks and the change in peak intensity for AgNPs within the same sample refer to the variation in the size of AgNPs inside the hydrogel matrix. The X-ray fluorescence (XRF) analysis revealed the elemental composition of the hydrogel samples. Table 2 illustrates the percentage composition of several elements within the hydrogel matrix across different concentrations of Ag. The quantities of Ag show variation in mass percentage (3.34%, 10.8%, 63.8%) for the three tested samples, NCH1, NCH2, and NCH4. The NCH4 sample showed the highest percentage of AgNPs compared to the other samples.

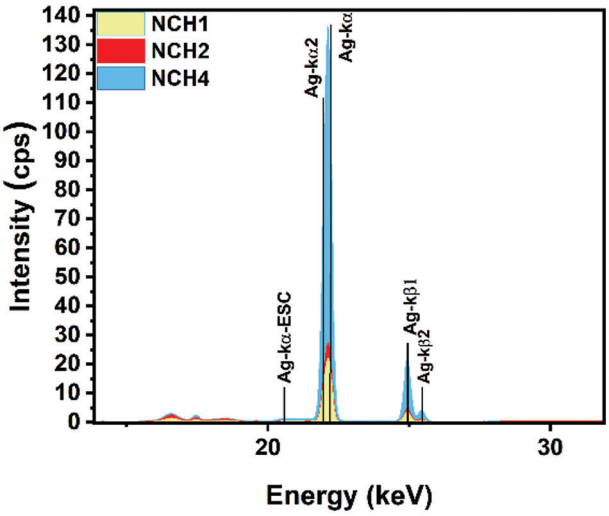

Figure 5: XRF analysis of NCH1, NCH2, and NCH4 samples

Table 2: Mass percentage of elemental in nanocomposite hydrogel samples determined by X-ray fluorescence (XRF) analysis

Sample	Cl (mass%)	Fe (mass%)	Ag (mass%)	K (mass%)
NCH1	9.17	17.2	3.34	10.4
NCH2	19.9	42.1	10.8	4.51
NCH4	0.88	0.62	63.8	10.1

Fig. 6 shows the nanoindentation test for two different samples, NCH2 and NCH3. The figure shows the effect of increasing Ag concentration on the hydrogel matrix. The array patterns were fixed for two samples to be 9-point with the same space distance (2 μm), with a fixed applied force of 500 μN. Fig. 6a,b shows a slight difference in curve shape indicating a change in the mechanical properties of samples with increasing Ag concentration.

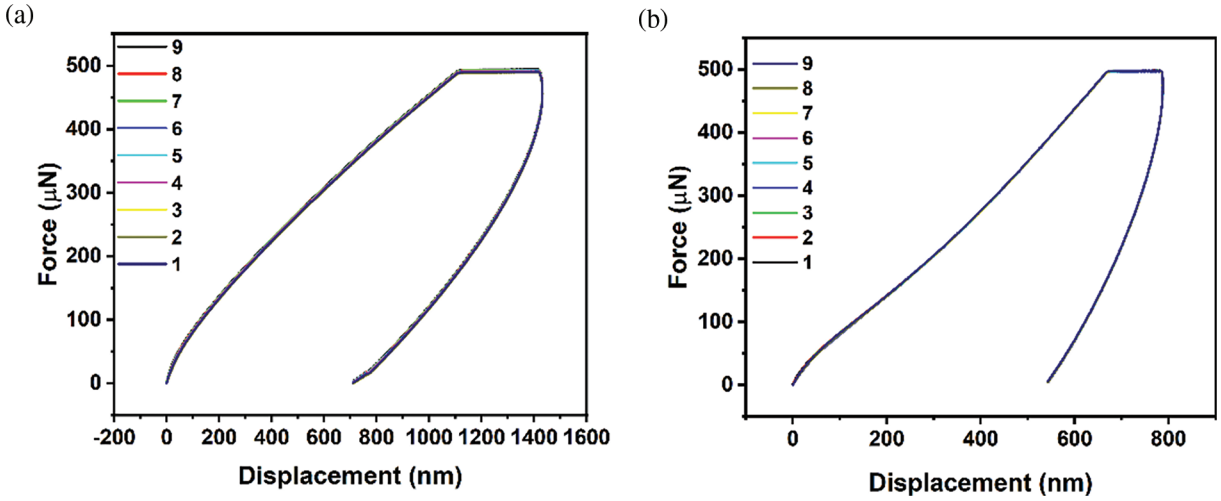

Figure 6: Scheme curve of nanoindentation load-displacement curve at nine different points for (a) NCH3 sample and (b) NCH2 sample passed on the 9-point array taken for the indentation test with a fixed distance

Table 3 shows the significant difference in standard deviation for both NCH3 and NCH2 samples, indicating a higher difference in sample mechanical properties. The NCH2 sample shows a higher standard deviation compared with the NCH3 sample for both hardness and elastic modulus. The Ag concentration plays an important role in increasing hydrogel mechanical properties. Sample NCH3 shows a lower elastic modulus and hardness value than the NCH2 sample.

Prepared hydrogels exhibited excellent swelling properties due to their porosity structure. The incorporation of AgNPs and RGO within the hydrogel matrix shows an increase in its porosity density as evidenced by SEM and AFM imaging, therefore increasing hydrogel swelling capability.

Fig. 7 illustrates the effect of concentrations of AgNP on the swelling capability of the hydrogel. Notably, the NCH3 sample with high AgNP concentration shows remarkable swelling capability.

Conversely, the H1 sample without AgNPs and RGO shows the lowest swelling capability compared to all other tested samples. The water content affords an interactive medium for charge transfer and ion diffusion in flexible energy storage devices. In addition, the surface properties and related electrochemical activity of hydrogel can be improved throughout swelling. Fig. 8 shows the cyclic voltammetry (CV) of hydrogel electrodes operated in a voltage window of –0.2 to 0.6 V. Fig. 8a shows the behavior of the (H1, NCH2, NCH3) sample working electrode in HCl as an acidic supporting electrode with a PH of 2.2. The current density of the hydrogel electrode shows significant differences between the H1 sample and the nanocomposite hydrogel (NCH3 and NCH2) samples, which refers to the effect of RGO and AgNPs on increasing the hydrogel conductivity and porosity. As a result, the diffusion channel resulting from high hydrogel porosity will allow electrolyte ions to transfer effectively. The CV curve of the H1 sample was included in the *Y*-axis, which refers to the insufficient intrusion of electrolyte ions into the hydrogel network and the increased hydrogel resistance. The effect of increasing AgNP concentration was also investigated.

Table 3: The differences in mechanical properties of NCH2 and NCH3 samples

Variables name	NCH2 sample	NCH3 sample
Hardness standard deviation	0.0070	0.0005
Elastic modulus standard deviation	0.1023	0.0039
Hardness	0.0221	0.0092
Elastic modulus	0.5794	0.1319

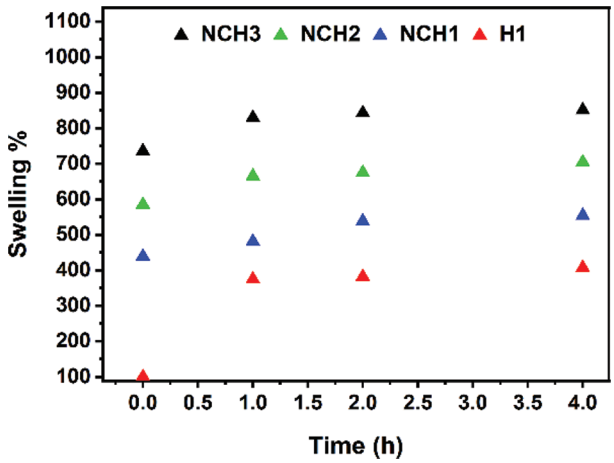

Figure 7: Swelling ratio of (H1, NCH1, NCH2, NCH3) samples

The NCH3 sample has a high content of AgNPs compared to the other samples, as seen in Fig. 8a, implying an improvement in their ionic conductivity supported by the porosity of the hydrogel matrix. Fig. 8b shows a multi-cycle scan to determine the electrochemical stability of the NCH3 sample. The NCH3 sample retains high capacitive storage. The strong electrochemical peak associated with redox and oxidation chemical reactions takes place at the electro-active species at the electrolyte/electrode interface.

The electrochemical performances of as-deposited flexible electrodes coincide with those of solid polymer electrolytes were also studied. Fig. S2a illustrates the time variation of current density for

H1, NCH1, NCH2, and NCH3 solid polymer electrode devices. The H1 electrode devices tend to have a low current density compared with other nanocomposite hydrogel electrodes. Hereby, the notable performance of flexible electrodes is assigned to integrating the RGO and Ag NPs into the hydrogel matrix, which results in higher ionic conductivity. The higher ratio of these additives plays a significant role in better electrode performance, while the dispersion and loading of this material can result in varying performance.

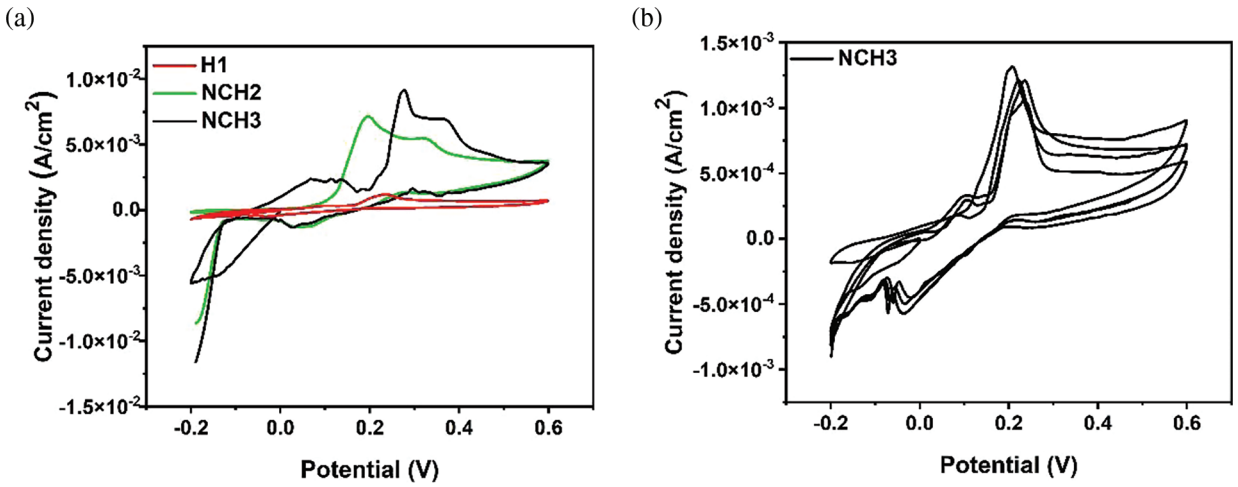

Figure 8: (a) The cyclic voltammetry curve of the H1, NCH2, and NCH3 samples, (b) The cyclic voltammetry curve of the NCH3 sample at four cycles

The solid structure of hydrogel in its dried state will increase hydrogel resistance. The CV curve of H1, NCH1, NCH2, and NCH3 solid electrolyte devices was measured in a potential range between (–0.2–0.6) V at a 100 mV/s scan rate. The CV for solid electrolytes shows a rectangular shape that comes close to the ideal electronic double-layer capacitor. The CV enclosed area differs with additive concentrations of RGO and Ag-NPs, which in turn will affect the energy stored in the flexible electrode. This finding implies that the large surface area of RGO can assist in energy storage in the hydrogel matrix (Fig. S2b).

In the last case, to quantify the wet surface properties on the performance of a flexible electrode device. The hydrogel was allowed to swell in deionized water before being used as an electrolyte. The device was constructed of an NCH4 sheet sample on one side of the supercapacitor, where the hydrogel was sandwiched between two ITO/PET flexible substrates, as shown in Fig. S1b. Fig. 9a–d represents the CV scan at 100 mV/s for different electrolyte samples. Interestingly, the capacitive energy storage can improve with increases in the additive ratios in nanocomposite hydrogel electrolytes. A higher water content in the hydrogel electrolyte after swelling leads to enhanced electrochemical performance of flexible electrode devices. The pseudocapacitive behavior was observed after swelling, suggesting the mechanism of charge storage can be tuned from double-layer performance to pseudocapacitive. At higher contents of RGO and AgNPs, stable electrochemical performance was observed due to efficient charge transfer and ion diffusion within the hydrogel matrix. The stability of the supercapacitor was demonstrated through consistent performance across multiple cycles, as observed in samples NCHS2 and NCHS3, which underwent many cycles with similar results (Fig. S3).

Fig. 10a,b shows the current and potential response curves with the time of the NCHS3 sample. The triangle shape of these curves is strongly believed to match the ideal supercapacitor. A stable performance with time variation was confirmed for the NCHS3 electrode device.

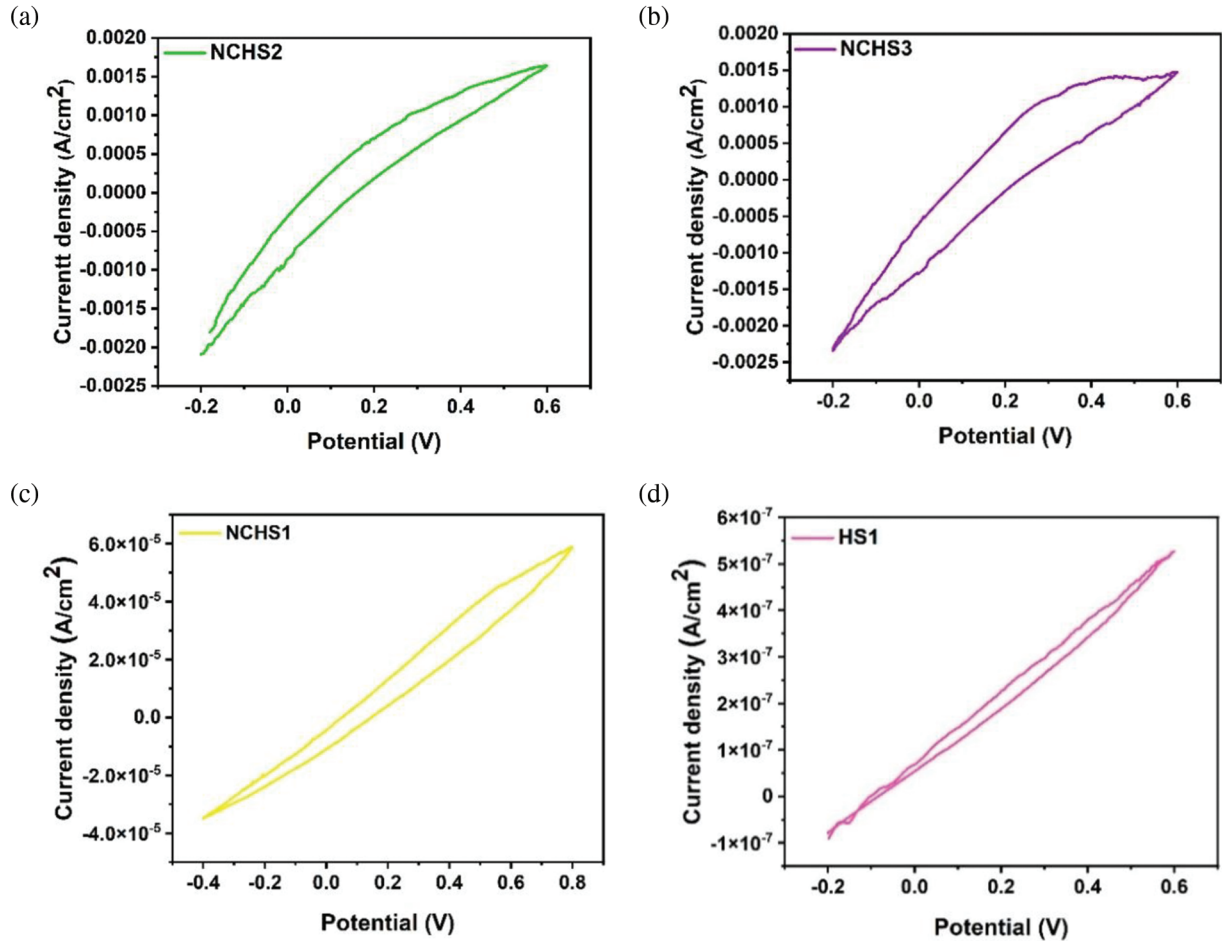

Figure 9: The cyclic voltammetry curve of the (a) NCHS2, (b) NCHS3, (c) NCHS1, and (d) HS1 samples

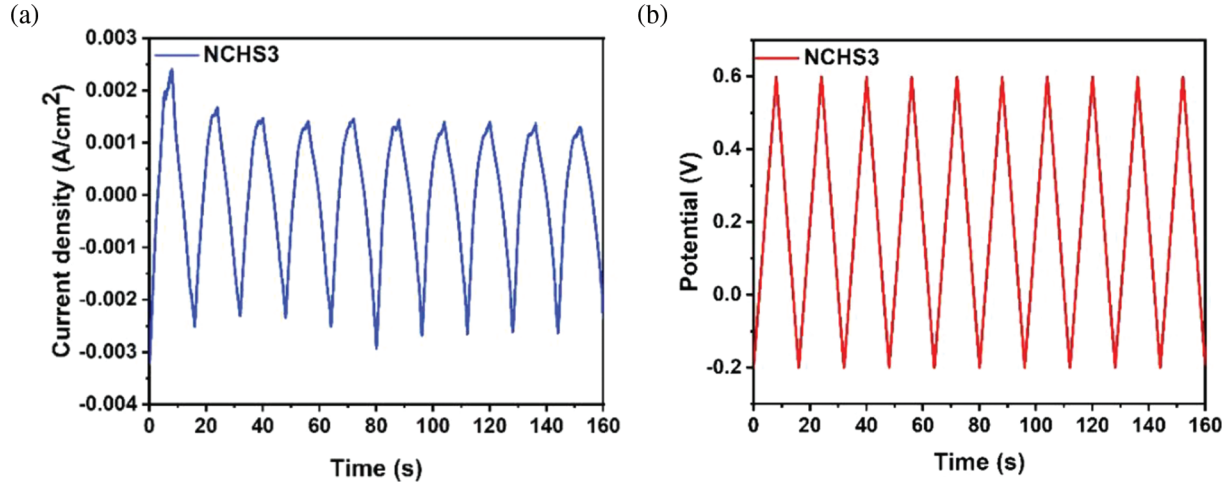

Figure 10: The plot of (a) current density and (b) potential difference *vs*. time for the NCHS3 sample

Fig. 11a–d elucidates the CV curves for both solid and gel polymer electrolytes at several scan rates (20–100) mV/s within the potential window of –0.2–0.6 V. The typical double-layer capacity coincides with the rectangular shape of a solid polymer electrolyte, as seen in Fig. 11a. On the other hand, the pseudocapacitive mechanism governed by semi-rectangular curves corresponding to the gel electrolyte polymer is shown in Fig. 11b. The energy storage mechanism converts from DLC to pseudocapacitive, suggesting efficient energy storage due to well-dispersed RGO and AgNPs. A stable performance at high scan rates was observed for both polymer electrolytes. Fig. 11c,d shows the effect of water content on the current density, as a result, gel-polymer electrolyte shows a higher current density than solid electrolyte. The figure shows the stability of the current density of the NCH3 sample compared with the NCHS3 sample, which indicates the smooth transport of ions inside the hydrogel matrix of the NCH3 sample.

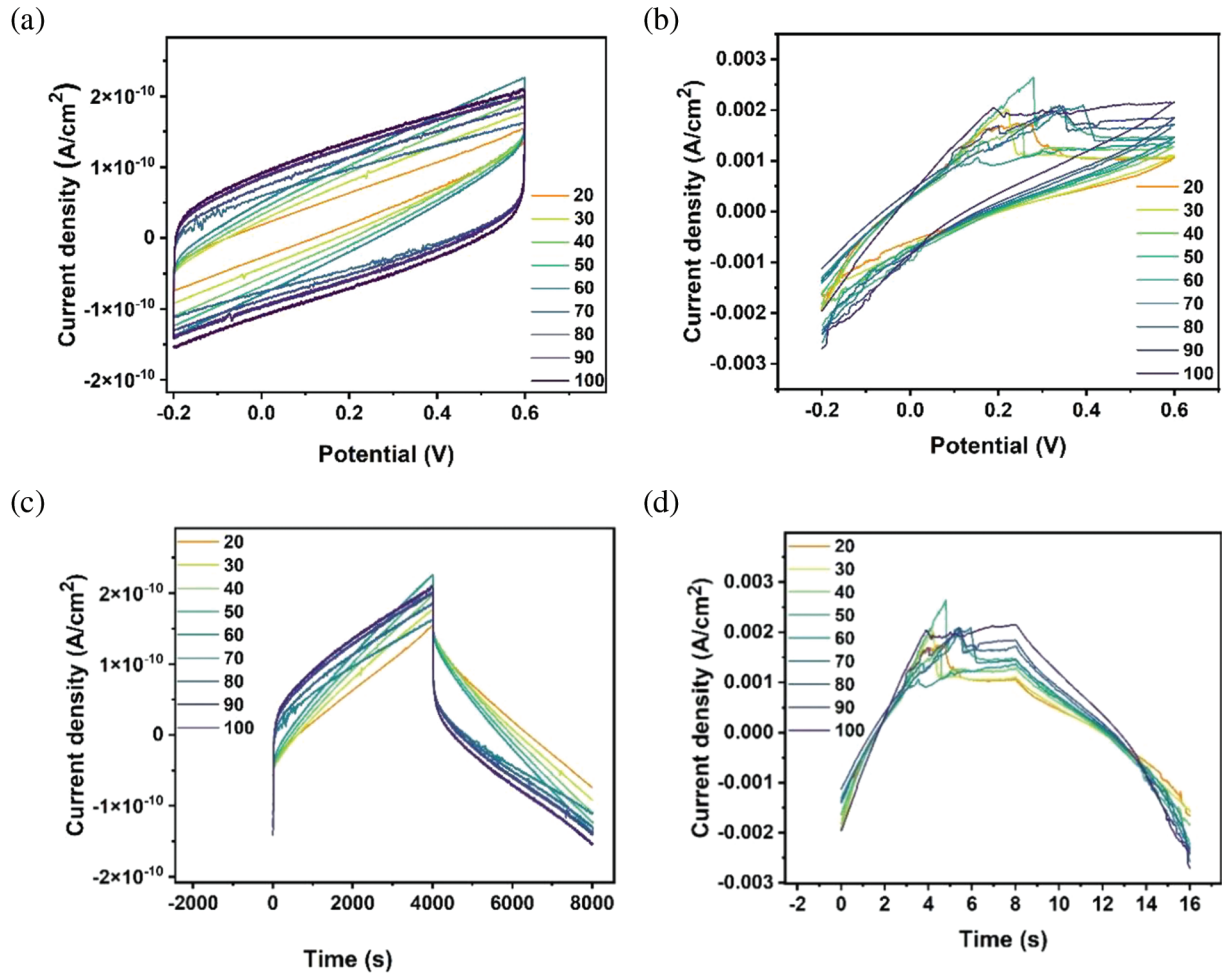

Figure 11: Cyclic voltammetry of (a) The NCH3 sample and (b) The NCHS3 sample at different scan rates. Current density to time plot of (c) The NCH3 sample and (d) The NCHS3 sample

The EIS was carried out to determine the charge transfer and ion diffusion of electro-chemicals with hydrogel matrix. The nyquist plot reveals significant differences between the NCH3 (Fig. 12a) and NCHS3 (Fig. 12b) samples. In addition, the increase in the electrical conductivity of flexible electrode devices improved with increases in the ratio of RGO and AgNP additives. Fig. 12c shows the difference in specific capacitance (Cs) between NCH3 and NCHS3 samples. The increase in Cs of the

NCHS3 sample compared with that of the NCH3 sample results from improved ion insertion on the hydrogel surface. Furthermore, the evaluated specific capacitances (Cs) for NCH3 and NCHS3 samples are compared to verify the influence of several additives in the hydrogel matrix. The efficient charge storage is confirmed by the Cs of the NCHS3 sample. This excellent performance assigned to several parameters can be epitomized as efficient charge transfer due to water content, RGO, AgNP additives, and large surface area. In addition, the smoothness of ion diffusion within the hydrogel matrix.

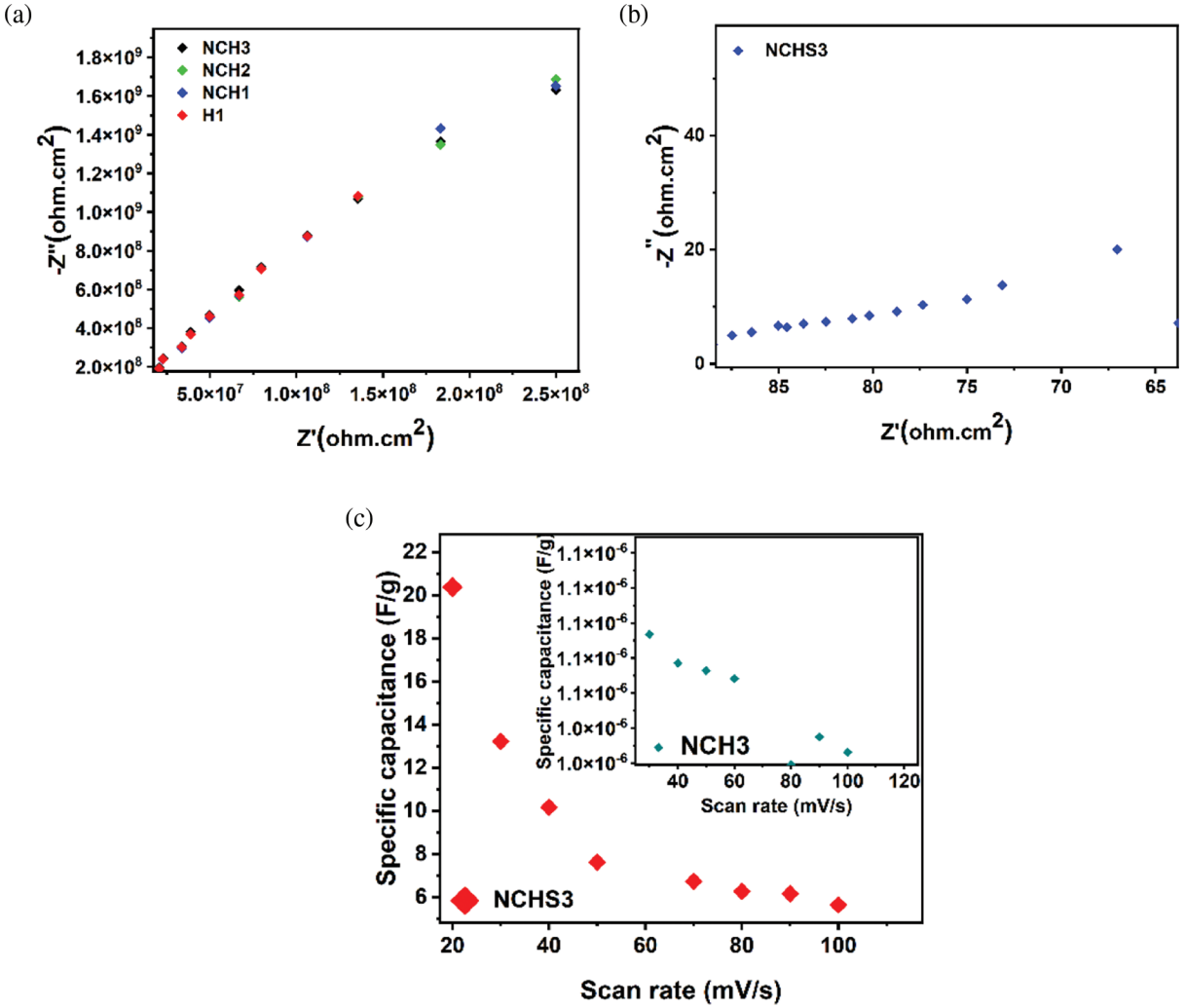

Figure 12: EIS plot for (a) H1, NCH1, NCH2, and NCH3 and (b) NCHS3 samples, (c) Specific capacitance of NCHS3 (red) and NCH3 (blue)

Fig. 13 illustrates the exceptional flexibility of the nanocomposite hydrogel structure. The image demonstrates its resilience against various mechanical stresses, including tension, crimping, knotting, and bending, without experiencing any cracking or tearing. This classification further emphasizes the robustness and elasticity of the hydrogel under applied loads, reflecting its suitability for flexible and durable supercapacitors.

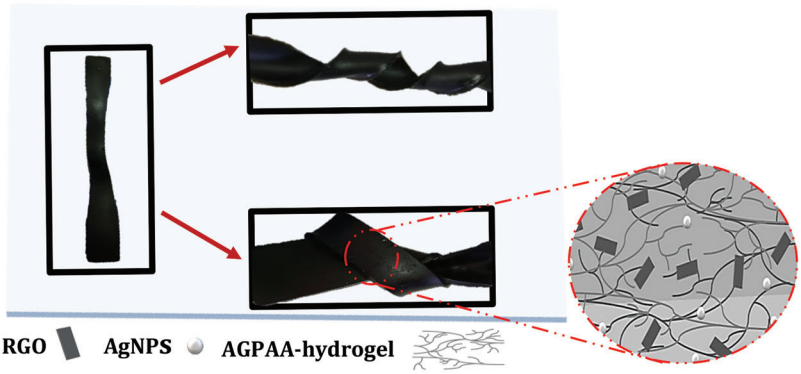

Figure 13: Mechanical properties of the nanocomposite hydrogel twisting and knotting

4 Conclusion

In summary, the advanced nanocomposite hydrogel matrix was synthesized by a physically cross-linked polymerization reaction of AG, AA, and Fe^{+3} ions. The hydrogel flexible electrode for supercapacitor devices was investigated. The device exhibits excellent mechanical and electrical properties under different conditions in dry and swelling environments. The high sensitivity of the hydrogel matrix to water content significantly improves the specific capacitance up to 20.0 F/g. The quite good performance is associated with the presence of RGO and AgNP additives in the hydrogel matrix, resulting in higher electrical conductivity. Additionally, the nanocomposite hydrogel was successfully utilized as a working electrode in HCl acidic electrolyte solution. The relatively high swelling capability, with higher RGO and AgNP contents at large surface structures, enables higher device performance. This result was confirmed by SEM, FTIR, XRF, AFM, and electrochemical performance. Consequently, high ionic mobility also enhances the energy storage efficiency of flexible hydrogel-based flexible supercapacitors. The prepared nanocomposite hydrogel may be used as a potential candidate for other energy-harvesting devices.

Acknowledgement: None.

Funding Statement: The authors are grateful for the Jordan University of Science and Technology's financial support for this research. This research was conducted under Grant No. 20230333.

Author Contributions: The authors confirm their contribution to the paper as follows: study conception and design: Borhan Albiss, Asala Saleh; data collection: Asala Saleh; analysis and interpretation of results: Borhan Albiss, Asala Saleh; draft manuscript preparation: Borhan Albiss, Asala Saleh. All authors reviewed the results and approved the final version of the manuscript.

Availability of Data and Materials: Data is available on request from the authors. The data supporting this study's findings are available from the corresponding author, Borhan Albiss, upon reasonable request.

Conflicts of Interest: The authors declare that they have no conflicts of interest to report regarding the present study.

Supplementary Materials: The supplementary material is available online at https://doi.org/10.32604/jrm.2024.050685.

References

1. Gupta A, Sardana S, Dahiya S, Punia R, Maan AS, Singh K, et al. Binder-free polypyrrole/fluorinated graphene nanocomposite hydrogel as a novel electrode material for highly efficient supercapacitors. Appl Surf Sci Adv. 2022;11:100297.
2. Zhu X, Jiang G, Wang G, Zhu Y, Cheng W, Zeng S, et al. Cellulose-based functional gels and applications in flexible supercapacitors. Resour Chem Mater. 2023;2:177–88. doi:10.1016/j.recm.2023.03. 004.
3. Zhang S, Zhao B, Zhang D, Yang M, Huang X, Han L, et al. Conductive hydrogels incorporating carbon nanoparticles: a review of synthesis, performance and applications. Particuology. 2023;83:212–31.
4. Wang J, Chen H, Xiao Y, Yu X, Li X. PAMPS/PVA/MMT semi-interpenetrating polymer network hydrogel electrolyte for solid-state supercapacitors. Int J Electrochem Sci. 2019;14:1817–29.
5. Li X, Wang Y, Li D, Shen C, Chen M, Long S, et al. Tough, flexible, and durable all-polyampholyte hydrogel supercapacitor. Polym Test. 2022;115:107720.
6. Simon SM, Prakashan VP, Sajna MS, Chandran A, George G, Barmiah EK, et al. Development and characterizations of Ag nanoparticles decorated TiO_2-ZrO_2 coatings as electrode material for supercapacitors. Results Surf Interfaces. 2023;10:100098.
7. Ullah R, Khan N, Khattak R, Khan M, Khan MS, Ali OM, et al. Preparation of electrochemical supercapacitor based on polypyrrole/gum Arabic composites. Polymers. 2022;14:242.
8. Guo G, Sun H, Sun Y, Li M. Facile synthesis of new conductive hydrogels for application in flexible all-solid-state supercapacitor. Int J Electrochem Sci. 2022;17:220528.
9. Bu X, Wu L, Ma X, Diao W, Lu D. Ultratough and reversibly stretchable zwitterionic poly(ionic liquid) copolymer hydrogel with high ionic conductivity for high-performance flexible and cold-resistant supercapacitor. Int J Electrochem Sci. 2020;15:2070–88.
10. Xu J, Jin R, Ren X, Gao G. A wide temperature-tolerant hydrogel electrolyte mediated by phosphoric acid towards flexible supercapacitors. Chem Eng J. 2021;413:127446.
11. Yang K, Fan Q, Song C, Zhang Y, Sun Y, Jiang W, et al. Enhanced functional properties of porous carbon materials as high-performance electrode materials for supercapacitors. Green Energy Resour. 2023;1:100030.
12. Pottathara YB, Tiyyagura HR, Ahmad Z, Sadasivuni KK. Graphene based aerogels: fundamentals and applications as supercapacitors. J Energy Storage. 2020;30. doi:10.1016/j.est.2020.101549.
13. Taş Ö., Kudaş Z, Ekinci KD. Electrochemical performance of diazonium-generated carbon films for electrochemical double-layer capacitors (EDLCs). Diam Relat Mater. 2023;138:110227. doi:10.1016/j.diamond. 2023.110227.
14. Shen H, Zhu Y, Zada I, Li H, Bokhari SW, Zhu S, et al. Investigation of strategies for improving the energy density of symmetric electrical double-layer capacitors. J Energy Storage. 2024;79. doi:10.1016/j.est.2023.110127.
15. Zhu X. Recent advances of transition metal oxides and chalcogenides in pseudo-capacitors and hybrid capacitors: a review of structures, synthetic strategies, and mechanism studies. J Energy Storage. 2022;49. doi:10.1016/j.est. 2022.104148.
16. Zhao J, Burke AF. Electrochemical capacitors: materials, technologies and performance. Energy Storage Mater. 2021;36:31–55. doi:10.1016/j.ensm.2020.12. 013.
17. Kraiwattanawong K. A review on the development of a porous carbon-based as modeling materials for electric double layer capacitors. Arab J Chem. 2022;15. doi:10.1016/j.arabjc.2021.103625.
18. Moya AA. Nonlinear charge-voltage relationships in electric double layer capacitors performing under constant load resistance. J Energy Storage. 2023;71:108136.
19. Wang J, Yu X, Wang C, Xiang K, Deng M, Yin H. PAMPS/MMT composite hydrogel electrolyte for solid-state supercapacitors. J Alloys Compd. 2017;709:596–601.
20. Zhang D, Sun B, Huang H, Gan Y, Xia Y, Liang C, et al. A solar-driven flexible electrochromic supercapacitor. Materials. 2020;13:1206.
21. Sudheer S, Bandyopadhyay S, Bhat R. Sustainable polysaccharide and protein hydrogel-based packaging materials for food products: a review. Int J Biol Macromol. 2023;248. doi:10.1016/j.ijbiomac.2023. 125845.

22. Mehrjou A, Hadaeghnia M, Ehsani Namin P, Ghasemi I. Sodium alginate/polyvinyl alcohol semi-interpenetrating hydrogels reinforced with PEG-grafted-graphene oxide. Int J Biol Macromol. 2024. doi:10.1016/j.ijbiomac.2024.130258.
23. El Fadl FIA, Hegazy DE, Maziad NA, Ghobashy MM. Effect of nano-metal oxides (TiO_2, MgO, CaO, and ZnO) on antibacterial property of (PEO/PEC-*co*-AAm) hydrogel synthesized by gamma irradiation. Int J Biol Macromol. 2023;250:126248.
24. Lin X, Shi J, Meng G, Pan Y, Liu Z. Effect of graphene oxide on sodium alginate hydrogel as a carrier triggering release of ibuprofen. Int J Biol Macromol. 2024;260:129515.
25. Tang L, Wu P, Zhuang H, Qin Z, Yu P, Fu K, et al. Nitric oxide releasing polyvinyl alcohol and sodium alginate hydrogels as antibacterial and conductive strain sensors. Int J Biol Macromol. 2023;241:124564.
26. Zhao Y, Hao H, Song T, Wang X, Li C, Li W. High energy-power density Zn-ion hybrid supercapacitors with N/P co-doped graphene cathode. J Power Sources. 2022;521:230941.
27. Ge M, Hao H, Lv Q, Wu J, Li W. Hierarchical nanocomposite that coupled nitrogen-doped graphene with aligned PANI cores arrays for high-performance supercapacitor. Electrochim Acta. 2020;330:135236.
28. Li H, Lv T, Sun H, Qian G, Li N, Yao Y, et al. Ultrastretchable and superior healable supercapacitors based on a double cross-linked hydrogel electrolyte. Nat Commun. 2019;10:5310.
29. Wang H, Zhao W. Application of hydrogel for energy storage and conversion. Next Mater. 2023;1:100049.
30. Quan LH, Thuy UTD, Nam PV, Chi NV, Duong TX, Hoa NV, et al. Chitosan-derived carbon aerogel nanocomposite as an active electrode material for high-performance supercapacitors. J Sci Adv Mater Dev. 2023;8:100586.
31. Khan M, Shah LA, Khan MA, Khattak NS, Zhao H. Synthesis of an un-modified gum arabic and acrylic acid based physically cross-linked hydrogels with high mechanical, self-sustainable and self-healable performance. Mater Sci Eng C. 2020;116:111278.
32. Cao X, Jiang C, Sun N, Tan D, Li Q, Bi S, et al. Recent progress in multifunctional hydrogel-based supercapacitors. J Sci Adv Mater Dev. 2021;6:338–50. doi:10.1016/j.jsamd.2021.06.002.
33. Li L, Xiang F, Wang F, Liu Y. Preparation and antitumor study of intelligent injectable hydrogel: carboxymethyl chitosan-aldehyde gum Arabic composite graphene oxide hydrogel. Int J Biol Macromol. 2024;259:129429.
34. Sultan M, Mohamed OA, El-Masry HM, Taha G. Fabrication and evaluation of antimicrobial cellulose/Arabic gum hydrogels as potential drug delivery vehicle. Int J Biol Macromol. 2023;242:125083.
35. de Souza AG, Cesco CT, de Lima GF, Artifon SES, Rosa DS, Paulino AT. Arabic gum-based composite hydrogels reinforced with eucalyptus and pinus residues for controlled phosphorus release. Int J Biol Macromol. 2019;140:33–42.
36. Wolf M, Gasparin BC, Paulino AT. Hydrolysis of lactose using β-D-galactosidase immobilized in a modified Arabic gum-based hydrogel for the production of lactose-free/low-lactose milk. Int J Biol Macromol. 2018;115:157–64.
37. Hassanzadeh-Afruzi F, Maleki A, Zare EN. Efficient remediation of chlorpyrifos pesticide from contaminated water by superparamagnetic adsorbent based on Arabic gum-grafted-polyamidoxime. Int J Biol Macromol. 2022;203:445–56.
38. Jalali ES, Shojaosadati SA, Hamedi S. Green synthesis of bovine serum albumin/oxidized gum Arabic nanocomposite as pH-responsive carrier for controlled release of piperine and the molecular docking study. Int J Biol Macromol. 2023;225:51–62.
39. Rajabi H, Jafari SM, Feizy J, Ghorbani M, Mohajeri SA. Preparation and characterization of 3D graphene oxide nanostructures embedded with nanocomplexes of chitosan- gum Arabic biopolymers. Int J Biol Macromol. 2020;162:163–74.
40. Gils PS, Ray D, Sahoo PK. Designing of silver nanoparticles in gum arabic based semi-IPN hydrogel. Int J Biol Macromol. 2010;46:237–44.
41. Gouda M, Khalaf MM, Abou Taleb MF, Abd El-Lateef HM. Fabrication of silver nanoparticles loaded acacia gum/chitosan nanogel to coat the pipe surface for sustainable inhibiting microbial adhesion and biofilm growth in water distribution systems. Int J Biol Macromol. 2024;262:130085.

42. Li S, Tao Y, Wu Y, Zhu S, Khademi S, Lv Y, et al. PANI/rGO−PAM/PVA hydrogels with applications in supercapacitive. J Polym Res. 2023;31:69. doi:10.21203/rs.3.rs-3391004/v1.
43. Fei L, Lin Q, Yuan B, Chen G, Xie P, Li Y, et al. Reduced graphene oxide wrapped fes nanocomposite for lithium-ion battery anode with improved performance. ACS Appl Mater Interfaces. 2013;5:5330–5.
44. Sun YA, Chen LT, Hsu SY, Hu CC, Tsai DH. Silver nanoparticles-decorating manganese oxide hybrid nanostructures for supercapacitor applications. Langmuir. 2019;35:14203–12.
45. Kalambate PK, Dar RA, Karna SP, Srivastava AK. High performance supercapacitor based on graphene-silver nanoparticles-polypyrrole nanocomposite coated on glassy carbon electrode. J Power Sourc. 2015;276:262–70.
46. Salve M, Mandal A, Amreen K, Pattnaik PK, Goel S. Greenly synthesized silver nanoparticles for supercapacitor and electrochemical sensing applications in a 3D printed microfluidic platform. Microchem J. 2020;157:104973.
47. Khamlich S, Khamliche T, Dhlamini MS, Khenfouch M, Mothudi BM, Maaza M, et al. Rapid microwave-assisted growth of silver nanoparticles on 3D graphene networks for supercapacitor application. J Colloid Interface Sci. 2017;493(14):130–7.
48. Alam SN, Sharma N, Kumar L. Synthesis of graphene oxide (GO) by modified hummers method and its thermal reduction to obtain reduced graphene oxide (rGO)*. Graphene. 2017;6:1–18.
49. Khan M, Shah LA, Rehman T, Khan A, Iqbal A, Ullah M, et al. Synthesis of physically cross-linked gum Arabic-based polymer hydrogels with enhanced mechanical, load bearing and shape memory behavior. Iran Polymer J. 2020;29:351–60.